

14. Bending of Wide Thick Mild Steel Plate

Junkichi YAGI*, *Member* and Toshihiko FUNAKI*, *Member*

(From *J.S.N.A. Japan*, Vol. 135, June 1974, Vol. 136, Dec. 1974 and Vol. 137, June 1975)

Summary

Main purposes of this work are to clarify mechanism of large bending deformation, and condition of bending crack initiation and also to propose a new practical method of bending test for industrial use.

In order to analyse large bending deformations of wide and narrow thick steel plates, analytical methods for bending of thick plates in the plane strain state and in the plane stress state were derived and calculated bending strains were compared to experimental results with good agreement.

On the other hand, many bending tests under uniform bending load and concentrated load were carried out and results were analysed by the methods and the condition of bending crack initiation was discussed.

Based on the above results, a new reasonable method of bending test for thick steel plate was proposed.

1. Introduction

Many industrial bending tests have been carried out to examine the ductility of materials, but these tests, for example JIS or ASTM standards, seem to be developed by experience and have some unreasonable points and establishment of more reasonable method is desired.

Research about bending crack initiation is quite few and there is only one research¹⁾ by Sangdahl and Sachs and they concluded that initiation of bending crack was affected by the biaxiality of stress distribution on surface of bent plate.

In order to investigate the condition of bending crack initiation more precisely, analytical method for large plastic deformations of thick plates were derived and differences in bending strain and stress distributions between the plane strain state and the plane stress state were clarified by the methods.

As a result of the analysis, it was found that for the same bending strain, circumfer-

ential bending stress in the plane strain state is a little larger than that in the plane stress state. Therefore bending crack initiates always in the middle part of plate whose stress condition is the plane strain state.

To find a more reasonable bending test method for industrial purpose, many tests under concentrated load were carried out and effects of shape of test specimen and friction force between the specimen and support on the bending crack initiation were clarified, and relations between bending strain and bending angle and between maximum bending strain and ratio of plate thickness to head radius of mandrel etc. were obtained.

2. Theory of Large Deformation of Thick Plate under Uniform Bending Moment

Large uniform bending deformation of thick plate as shown in Fig. 1 is described exactly by the outward radial displacement U and the bending angle θ . The radial displacement and the tangential displacement U and V were used for analysis of plastic bending of thick plate but they can be used accurately only

* Osaka University

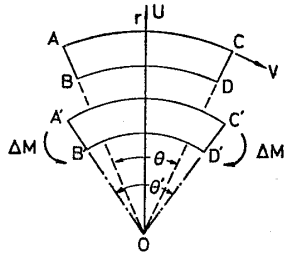


Fig. 1 Large bending deformation of thick plate

for small bending deformations. Using these displacements U and θ , nominal circumferential strain increment $\Delta\epsilon_\theta$ and radial strain increment $\Delta\epsilon_r$ due to increase in the bending angle can be written as

$$\left. \begin{aligned} \Delta\epsilon_\theta &= \frac{\widehat{A'C'} - \widehat{AC}}{\widehat{AC}} = \frac{\theta'}{\theta} \left\{ 1 + \frac{U}{r} \right\} - 1, \\ \Delta\epsilon_r &= \lim_{\overline{AB} \rightarrow 0} \frac{\overline{A'B'} - \overline{AB}}{\overline{AB}} = \frac{dU}{dr} \end{aligned} \right\} \quad (1)$$

2.1 Distribution of Uniform Bending Strain in the Plate Strain State

Bending radii r_b and r_a on surfaces of convex and concave side of thick plate and the bending angle θ change from some values (r_{bi}, r_{ai}, θ_i) at i -step to another values ($r_{bi+1}, r_{ai+1}, \theta_{i+1}$) at $i+1$ -step as indicated in Fig. 2.

The nominal bending strain increments on the surfaces of the plate between the two steps are given by eq. (2)

$$\Delta\epsilon_{\theta bi} = \frac{r_{bi+1}\theta_{i+1}}{r_{bi}\theta_i} - 1, \quad \Delta\epsilon_{\theta ai} = \frac{r_{ai+1}\theta_{i+1}}{r_{ai}\theta_i} - 1 \quad (2)$$

Assuming the condition of no change of volume, we find the following equation.

$$(r_{bi}^2 - r_{ai}^2)\theta_i = (r_{bi+1}^2 - r_{ai+1}^2)\theta_{i+1} \quad (3)$$

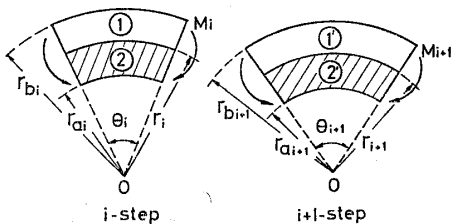


Fig. 2 Deformation at i and $i+1$ step of loading in the plane strain state

From eqs. (2) and (3), we have

$$\left. \begin{aligned} r_{bi+1} &= \frac{(r_{bi}^2 - r_{ai}^2)r_{bi}(1 + \Delta\epsilon_{\theta bi})}{r_{bi}^2(1 + \Delta\epsilon_{\theta bi})^2 - r_{ai}^2(1 + \Delta\epsilon_{\theta ai})^2} \\ r_{ai+1} &= \frac{(r_{bi}^2 - r_{ai}^2)r_{ai}(1 + \Delta\epsilon_{\theta ai})}{r_{bi}^2(1 + \Delta\epsilon_{\theta bi})^2 - r_{ai}^2(1 + \Delta\epsilon_{\theta ai})^2} \\ \theta_{i+1} &= \frac{r_{bi}^2(1 + \Delta\epsilon_{\theta bi})^2 - r_{ai}^2(1 + \Delta\epsilon_{\theta ai})^2}{r_{bi}^2 - r_{ai}^2} \theta_i \end{aligned} \right\} \quad (4)$$

From eqs. (2), (3) and (4), the following relations are obtained for the radii of an arbitrary fiber of the plate r_i at i -step and r_{i+1} at $i+1$ -step.

$$\begin{aligned} r_{i+1} &= \frac{(r_{bi}^2 - r_{ai}^2)}{r_{bi}^2(1 + \Delta\epsilon_{\theta bi})^2 - r_{ai}^2(1 + \Delta\epsilon_{\theta ai})^2} \cdot r_i(1 + \Delta\epsilon_{\theta i}) \\ &= \frac{(r_i^2 - r_{ai}^2)}{r_i^2(1 + \Delta\epsilon_{\theta i})^2 - r_{ai}^2(1 + \Delta\epsilon_{\theta ai})^2} \cdot r_i(1 + \Delta\epsilon_{\theta i}) \end{aligned} \quad (5)$$

From eq. (5) the nominal circumferential strain increment $\Delta\epsilon_{\theta i}$ of an arbitrary fiber at i -step can be written as eq. (6)

$$\Delta\epsilon_{\theta i} = \sqrt{B_i - \left(\frac{A_i B_i}{r_i}\right)^2} - 1 \quad (6)$$

where

$$\begin{aligned} A_i &= \frac{r_{ai}r_{bi}}{r_{bi}(1 + \Delta\epsilon_{\theta bi})^2 - r_{ai}(1 + \Delta\epsilon_{\theta ai})^2} \\ &\quad \times \sqrt{\frac{r_{bi}^2 - r_{ai}^2}{(1 + \Delta\epsilon_{\theta bi})^2 - (1 + \Delta\epsilon_{\theta ai})^2}} \\ B_i &= \frac{\theta_{i+1}}{\theta_i} \end{aligned}$$

Expanding eq. (6) into Taylor series and neglecting powers higher than 2 of small quantities, we have the same formula derived by Hill²⁾ and Schaffer³⁾ for small bending deformation.

2.2 Distribution of Uniform Bending Strain in the Plane Stress State

In case of the plane stress state, since longitudinal cross section of the plate, $r\theta$ plane, has no normal stress perpendicular to the plane, transverse cross section of the bent plate does not remain square.

In order to analyse bending deformation of thick plate in the plane stress state, we assume that ratio of breadth to thickness of the plate

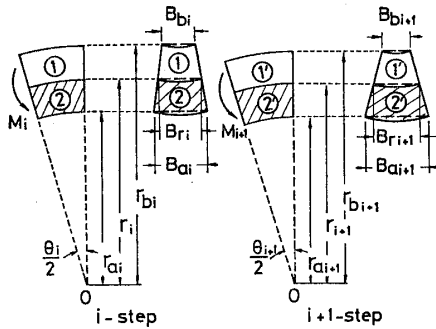


Fig. 3 Deformation at i and $i+1$ step of loading in the plane stress state

is very small and shape of the transverse cross section of the bent plate is approximately trapezoidal instead of fan shape as shown by dotted line in Fig. (3).

$$\left. \begin{aligned} r_{bi+1} &= r_{bi}(1 + \Delta\varepsilon_{\theta bi}) \frac{\theta_i}{\theta_{i+1}}, & r_{ai+1} &= r_{ai}(1 + \Delta\varepsilon_{\theta ai}) \frac{\theta_i}{\theta_{i+1}} \\ \frac{\theta_{i+1}}{\theta_i} &= \frac{\{r_{bi}(1 + \Delta\varepsilon_{\theta bi}) - r_{ai}(1 + \Delta\varepsilon_{\theta ai})\} \{(B_{bi+1} + 2B_{ai+1})r_{ai}(1 + \Delta\varepsilon_{\theta ai}) + (2B_{ai+1} + B_{ai+1})r_{bi}(1 + \Delta\varepsilon_{\theta bi})\}}{(r_{bi} - r_{ai}) \{(B_{bi} + 2B_{ai})r_{ai} + (2B_{bi} + B_{ai})r_{bi}\}} \\ B_{bi+1} &= B_{bi} \exp[\sqrt{(1 + \Delta\varepsilon_{\theta bi})}], & B_{ai+1} &= B_{ai} \exp[\sqrt{(1 + \Delta\varepsilon_{\theta ai})}] \end{aligned} \right\} \quad (8)$$

Considering the condition of continuity of strain at the boundary of upper and lower part ① and ② of cross section of the plate shown in Fig. 3, the following equation is obtained for bending radius r_i of an arbitrary fiber of the bent plate at i -step.

$$\begin{aligned} & 2P(C_{bi} + C_{ai})(1 + \Delta\varepsilon_{\theta i})^3 \\ & + [C_{bi}\{(B_{bi+1} + 2Q_i)r_i^2 - P_i r_{bi+1} r_i\} \\ & + C_{ai}\{(B_{ai+1} + 2Q_i)r_i^2 - P_i r_{ai+1} r_i\}](1 + \Delta\varepsilon_{\theta i})^2 \\ & + [C_{bi}\{(B_{bi+1} - Q_i)r_{bi+1} r_i - P_i r_{bi+1}^2\} \\ & + C_{ai}\{(B_{ai+1} - Q_i)r_{ai+1} r_i - P_i r_{ai+1}^2\}](1 + \Delta\varepsilon_{\theta i}) \\ & + C_{bi}(2B_{bi+1} + Q_i)r_{bi+1}^2 - C_{ai}(2B_{ai+1} + Q_i)r_{ai+1}^2 = 0 \end{aligned} \quad (9)$$

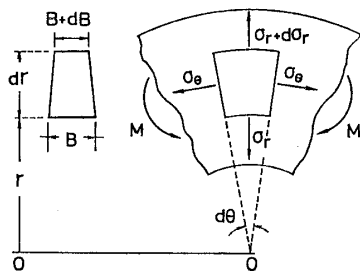


Fig. 4 Stress components in the bent plate

Using the above assumption, shape of the bent plate is described by the radius r_b , breadth B_b on convex surface, the radius r_a , breadth B_a on concave surface and the bending angle θ . From the condition of constant volume eq. (7), relations between these quantities at i -step and $i+1$ -step can be expressed by the strain increments $\Delta\varepsilon_{\theta bi}$ and $\Delta\varepsilon_{\theta ai}$ as eq. (8).

$$\begin{aligned} & \frac{B_{ai} + B_{bi}}{2} (r_{bi} - r_{ai}) \left(r_{ai} + \frac{r_{bi} - r_{ai}}{3} \frac{B_{ai} + 2B_{bi}}{B_{ai} + B_{bi}} \right) \theta_i \\ & = \frac{B_{ai+1} + B_{bi+1}}{2} (r_{bi+1} - r_{ai+1}) \\ & \times \left(r_{ai+1} + \frac{r_{bi+1} - r_{ai+1}}{3} \frac{B_{ai+1} + 2B_{bi+1}}{B_{ai+1} + B_{bi+1}} \right) \theta_{i+1} \end{aligned} \quad (7)$$

where

$$\begin{aligned} P_i &= \frac{B_{bi+1} - B_{ai+1}}{r_{bi+1} - r_{ai+1}} \cdot \frac{\theta_i}{\theta_{i+1}} \cdot r_i \\ Q_i &= B_{ai+1} - \frac{B_{bi+1} - B_{ai+1}}{r_{bi+1} - r_{ai+1}} r_{ai+1} \\ C_{bi} &= (2B_{ri} + B_{ai})r_i^2 + (B_{ai} - B_{ri})r_{ai}r_i \\ & \quad - (B_{ri} + 2B_{ai})r_{ai}^2 \\ C_{ai} &= (2B_{bi} + B_{ri})r_{bi}^2 + (B_{ri} - B_{bi})r_{bi}r_i \\ & \quad - (B_{bi} + 2B_{ri})r_{bi}^2 \\ B_{ri} &= B_{ai} + \frac{B_{bi} - B_{ai}}{r_{bi} - r_{ai}} (r_i - r_{ai}) \end{aligned}$$

Breadthwise strain increment $\Delta\varepsilon_{zi}$ on the fiber is $(B_{ri+1}/B_{ri}) - 1$ and the radial strain increment $\Delta\varepsilon_{ri}$ on the fiber is easily obtained from the condition of constant volume.

$$\Delta\varepsilon_{ri} = (1 + \Delta\varepsilon_{\theta i})(1 + \Delta\varepsilon_{zi})^{-1} - 1 \quad (10)$$

2.3 Equilibrium of Forces

Normal radial and circumferential stress components σ_r and σ_θ of the plate under uniform bending load are functions of radius r only and shearing stress component of the plate vanishes from the condition of symmetry, and

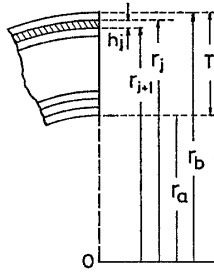


Fig. 5 Layers divided for numerical analysis

equilibrium equation of forces in the radial direction of the bent plate is

$$(\sigma_r + d\sigma_r)(r + dr)d\theta(B + dB) - \sigma_r r d\theta B = 2\sigma_\theta \frac{(2B + dB)dr}{2} d\theta \quad (11)$$

Neglecting small quantities higher than the second order, eq. (11) becomes

$$\frac{d}{dr}(\sigma_r r B) = \sigma_\theta B \quad (12)$$

In case of the plane stress state, breadth of the plate B changes with increase of load, but in case of the plane strain state the breadth does not change.

For numerical calculation, the plate is divided into N thin layers of equal thickness as shown in Fig. 5. When thickness of layer

$$\left. \begin{aligned} \text{for loading layers;} \quad & |\sigma_{\theta j} - \sigma_{rj}| = f_{\pm} \left(\frac{4}{3} |\bar{\epsilon}_{\theta j}| \right) && \text{(in the plane strain state)} \\ & |\sigma_{\theta j} - \sigma_{rj}| = f_{\pm} \left(\frac{2}{3} |\bar{\epsilon}_{\theta j} - \bar{\epsilon}_{rj}| \right) && \text{(in the plane stress state)} \\ \text{for unloading layers;} \quad & |\sigma_{\theta j} - \sigma_{rj}| = \sigma_y && \text{(in the plane strain state and} \\ & && \text{in the plane stress state)} \end{aligned} \right\} \quad (14-1)$$

When Mises' yield condition is applied, the following relations are given

$$\left. \begin{aligned} \text{for loading layers;} \quad & |\sigma_{\theta j} - \sigma_{rj}| = \frac{2}{\sqrt{3}} f_{\pm} \left(\frac{2}{\sqrt{3}} |\bar{\epsilon}_{\theta j}| \right) && \text{(in the plane strain state)} \\ & \sqrt{\sigma_{\theta j}^2 - \sigma_{\theta j} \sigma_{rj} + \sigma_{rj}^2} = f_{\pm} \left(\frac{2}{\sqrt{3}} \sqrt{(\bar{\epsilon}_{\theta j} - \bar{\epsilon}_{rj})^2 + (\bar{\epsilon}_{rj} - \bar{\epsilon}_{zj})^2 + (\bar{\epsilon}_{zj} - \bar{\epsilon}_{\theta j})^2} \right) && \text{(in the plane stress state)} \\ \text{for unloading layers;} \quad & |\sigma_{\theta j} - \sigma_{rj}| = \frac{2}{\sqrt{3}} \sigma_y && \text{(in the plane strain state)} \\ & \sqrt{\sigma_{\theta j}^2 - \sigma_{\theta j} \sigma_{rj} + \sigma_{rj}^2} = \sigma_y && \text{(in the plane stress state)} \end{aligned} \right\} \quad (14-2)$$

where f_+ means the equivalent stress-strain relation used for layers under tensile load and f_- means the one for layers under compressive load and σ_y is yield stress at i -step and $\bar{\epsilon}$ is logarithmic strain component.

h_j is very small compared with thickness of the plate T , eq. (13) can be used instead of eq. (12) with sufficient accuracy.

$$[\sigma_r r B]_{r_{j+1}}^{r_j} \doteq \sigma_{\theta j} \frac{B_j + B_{j+1}}{2} (r_j - r_{j+1}) \quad (13)$$

2.4 Loading and Unloading

With increase of bending deformation neutral surface of the bent plate moves to concave side. Equivalent strain in portions I and III in Fig. 6 increases with increase of bending load, but the strain in portion II decreases and unloading occurs.

Applying Tresca's yield condition to the work hardening behaviour of material, the following relations between σ_θ and σ_r are obtained.

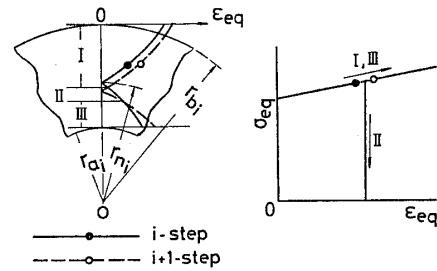


Fig. 6 Loading and unloading process

2.5 Boundary Condition

As the radial stresses σ_r on surfaces of the plate are always zero, the bending stresses σ_θ on the surfaces are determined by the total strain theory, if the strain components on the surfaces are given.

Fig. 7 indicates a flow chart for numerical analysis of bending in the plane strain state. When the bending radii r_{bi} , r_{ai} , the bending angle θ_i at i -step and the bending strain increments $\Delta\epsilon_{\theta bi}$, $\Delta\epsilon_{\theta ai}$ between i -step and $i+1$ -step are given, the strain distribution of the bent plate at $i+1$ -step can be determined from eq. (6) or (9) and stress distribution at $i+1$ -step may be determined from eqs. (13) and (14).

Ratio of the bending strain increments of

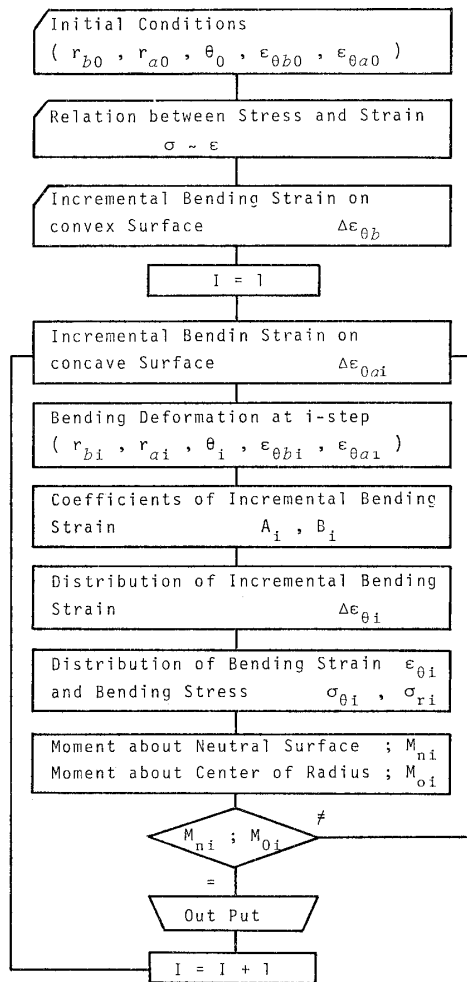


Fig. 7 Flow chart for numerical analysis

the surfaces $\Delta\epsilon_{\theta ai}/\Delta\epsilon_{\theta bi}$ should be determined by iteration method shown in Fig. 7 so as to satisfy the condition of no axial force, that is

$$M = \int_{r_a}^{r_b} \sigma_\theta r B dr = \int_{r_a}^{r_b} \sigma_\theta (r - r_n) B dr \quad (15)$$

where r_n is bending radius of neutral surface of the bent plate.

3. Results of Calculation

For numerical calculation, the plate was divided into 50 thin layers of equal thickness and the bending strain increment on convex surface $\Delta\epsilon_{\theta bi}$ between i -step and $i+1$ -step was assumed to be 0.005 and the increment on concave surface $\Delta\epsilon_{\theta ai}$ was determined so as to satisfy eq. (15) by the iteration method indicated in Fig. 7.

The equivalent stress-strain relation obtained from tensile test result of a thin steel plate was used for tensile part of the plate and the relation obtained from compressive test result of a solid cylindrical steel specimen was applied to compressive part of the plate.

Fig. 8 shows relation between the bending radius on convex surface r_b or the bending angle θ and the bending strain on convex surface $\epsilon_{\theta b}$ in the plane strain state. Fig. 9 illustrates relation between thickness of the plate T or the bending radius of the neutral surface r_n and the radius of convex surface r_b in the plane strain state.

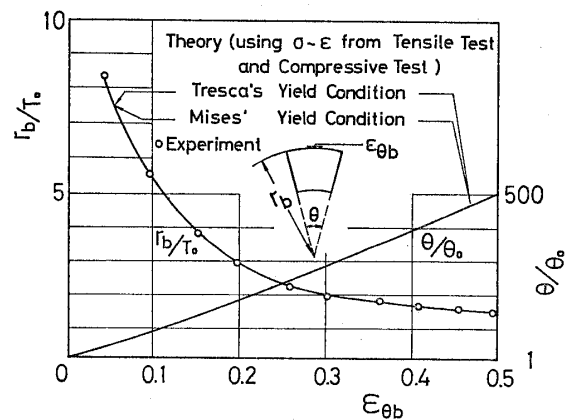


Fig. 8 Relation between bending radius or bending angle and circumferential strain in the plane strain state

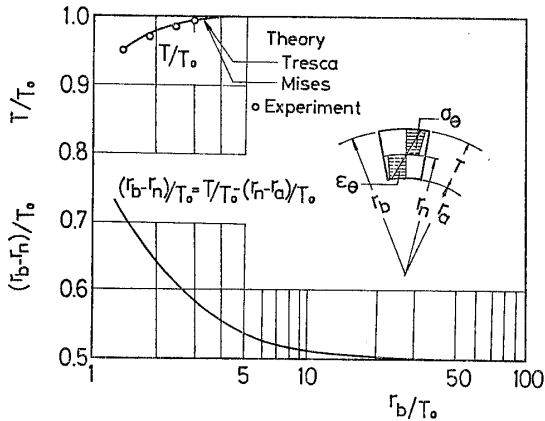


Fig. 9 Relation between thickness of plate or radius of neutral surface and radius on convex surface of plate in the plane strain state

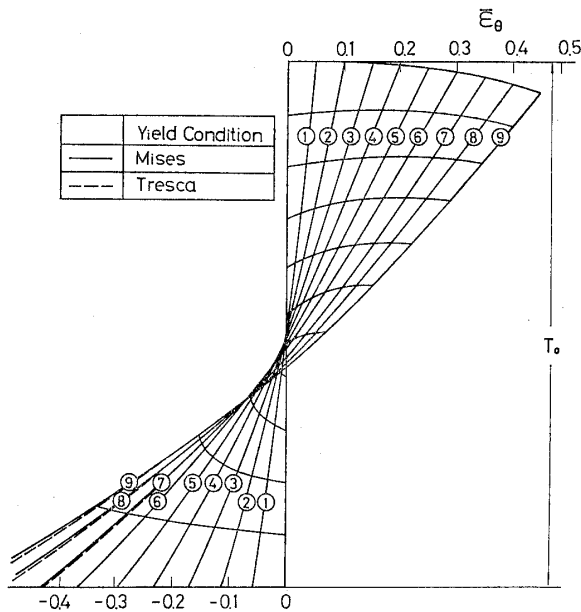


Fig. 10 Strain distribution in the plane strain state

As it is clear from Fig. 8 and 9, there are no distinct differences in bending deformation between the case based on Tresca's yield condition and the one based on Mises' yield condition. And there are also no large differences in the deformation between the two stress states with the exception of differences in the radius of the neutral surface.

Figs. 10 and 11 show typical examples of strain and stress distributions at each loading step on the longitudinal section of the plate

in the plane strain state.

From these figures, it is recognized that there are hardly any differences in the strain distribution between the two cases, but a little differences are found in the stress distribution and the stresses based on Mises'

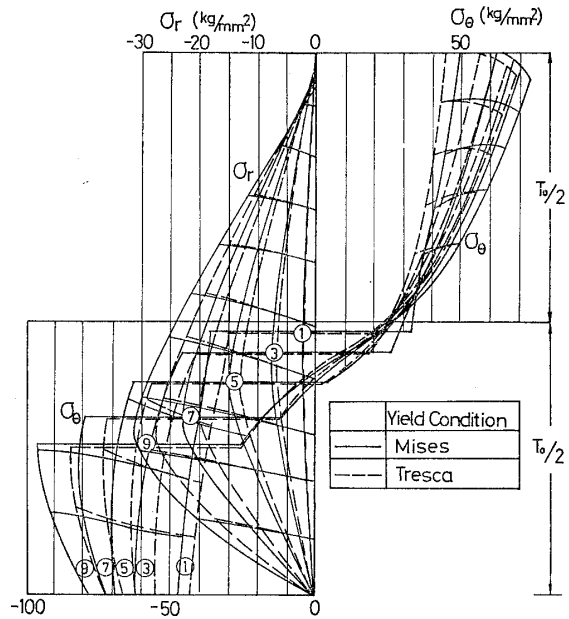


Fig. 11 Distributions of circumferential stress and radial stress in the plane strain state

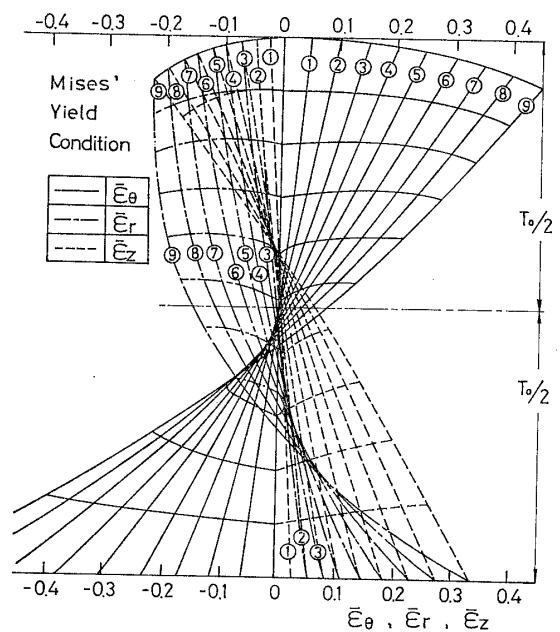


Fig. 12 Strain distribution in the plane stress state

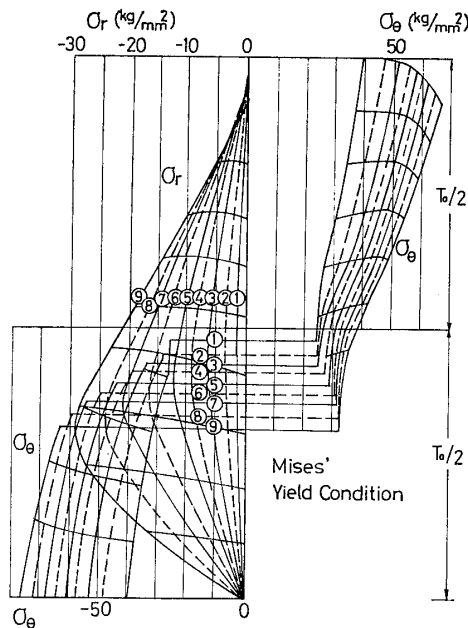


Fig. 13 Distributions of circumferential stress and radial stress in the plane stress state

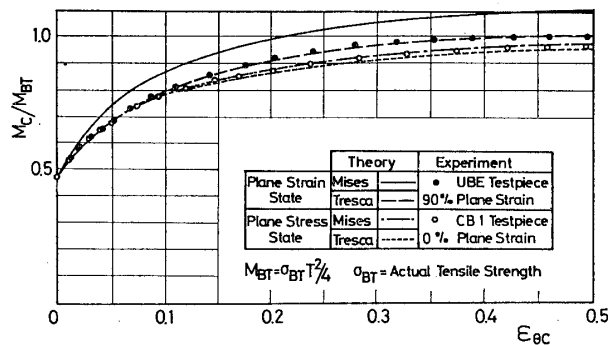


Fig. 14 Relation between bending moment and bending strain

yield condition are a little larger than those based on Tresca's yield condition, especially in the part of compressive side of the plate.

Figs. 12 and 13 show some examples of strain and stress distribution in the plane stress state. In this state, similar to the above examples, there are little differences in the strain distribution between the two cases, but in the stress distribution, the same tendency as in the case of the plane strain is found. Although the bending stresses based on Mises' yield condition are a little larger than those based on Tresca's one, there are negligible differences between two bending

moments calculated from the two stress distribution as in Fig. 14.

Fig. 14 shows relation between bending moments and bending strains. In case of plane strain state, bending moments calculated from the stress distribution based on Tresca's yield condition agree with experimental results with sufficient accuracy, but the moments based on Mises' yield condition is a little larger than experimental ones.

On the other hand, in case of plane stress state, the calculated bending moments based on the two yield conditions agree well with the test results.

4. Results of Bending Test

In order to verify the validity of the theory of bending derived in the previous section, bending tests under uniform bending load and concentrated load were carried out and test results were compared with the theoretical values.

On the other hand, influence of shape of test specimen and loading apparatus on the initiation of bending crack were discussed and a new practical bending test method was proposed.

4.1 Material

Material used for the bending tests is mild steel and its chemical compositions and mechanical properties are shown in Tables 1 and 2.

Table 1 Chemical compositions (%)

C	Si	Mn	P	S
0.17	0.02	1.09	0.012	0.017

Table 2 Mechanical properties

$\sigma_{1.5}$ (kg/mm ²)	σ_B (kg/mm ²)	E (kg/mm ²)	Φ (%)	δ (%)	ϵ_U (%)
25.5	43.9	21000	35.5	60.1	25.2

4.2 Test Specimen and Test Apparatus

a. Uniform bending test

Uniform bending tests were carried out under 4 point loads as shown in Fig. 15-1 for

comparatively small bending deformation and after the deformation reached to some limiting value, the specimen was bent by compressive load as illustrated in Fig. 15-2 until many bending cracks were observed.

In the later test, ratio of compressive stress to bending stress at middle section σ_c/σ_b is smaller than 5% and effect of compressive stress on the initiation of bending crack is considered to be negligible.

Shape and size of the specimens are shown in Fig. 17 and Table 3.

As breadth of middle part of UB-Type specimen is narrowed, bending deformation was concentrated mainly in this part and bending

Table 3 Size of specimen for uniform bending test

Type	L_0 (mm)	B_0 (mm)	b (mm)	b/T_0
UB 1		60.0	19.0	1.0
UB 3		180.0	57.0	3.0
UB 5	800.0	300.0	95.0	5.0
UB 8		480.0	152.0	8.0
UB 10		600.0	190.0	10.0
UBE	800.0	500.0	500.0	26.3

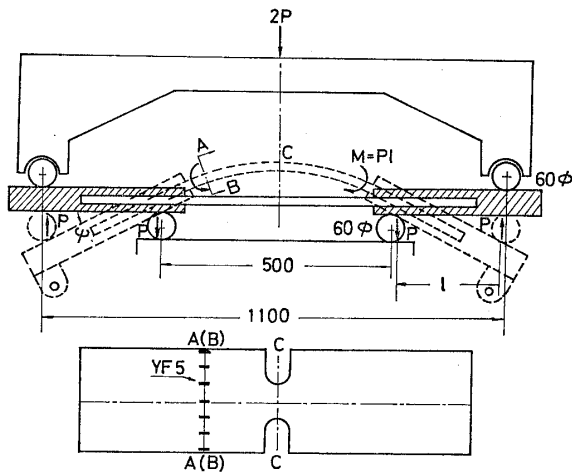


Fig. 15-1 Uniform bending test

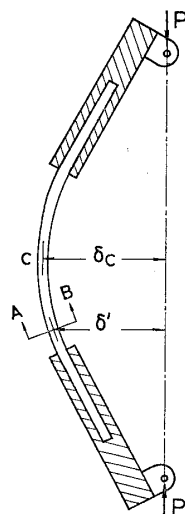


Fig. 15-2 Bending test under compressive load

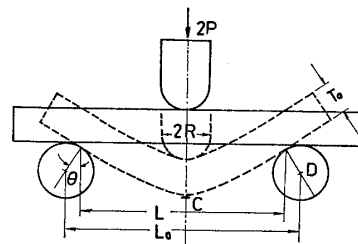


Fig. 16 Bending test under concentrated load

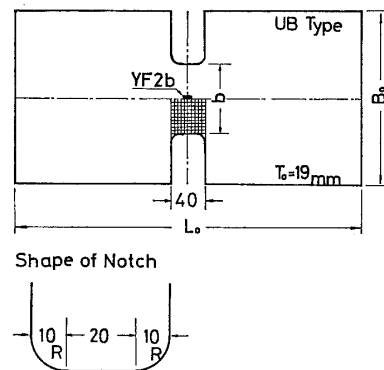


Fig. 17 Shape of test piece

cracks were found in this part. Breadth of UBE-Type specimen is very large and has no narrow part and region of the plane strain state was about 90% of breadth of the specimen.

b. Bending test under concentrated load

In order to develop a simple and practical bending test method, bending tests under concentrated load were carried out and test results were compared with those of uniform bending tests. The test method is shown in

Table 4 Size of specimen for bending test under concentrated load

Type	L_0 (mm)	B_0 (mm)	B_0/T_0
CB 1	104.0	19.0	1
CB 2A	230.0	38.0	2
CB 2B	180.0	38.0	2
CB 3	104.0	57.0	3
CB 5	104.0	95.0	5
CB 8	104.0	152.0	8
CB 10	104.0	190.0	10

Fig. 16 and shape and size of specimens are shown in Fig. 17 and Table 4.

4.3 Measurement of Bending Strain

For small deformation, bending strains were measured with strain gages and for large deformation, the strains were estimated from radius of curvature measured with a simple device shown in Fig. 18 and strain determined from change of space of grid printed on surface of specimen, that is, the bending strain on convex surface of specimen is calculated by the following equation.

$$\varepsilon_\theta = r_b \sin\left(\frac{S}{2r_b}\right) - 1 \quad (16)$$

where

- $r_b = \frac{W^2 + 4}{2W}$: radius of curvature on surface of specimen
- W : relative displacement between spindle of dial gage and fixed legs
- S : space of grid on sur-

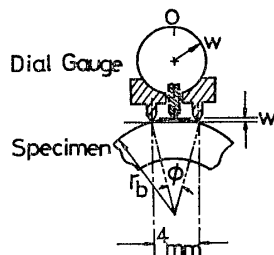


Fig. 18 Device for measurement of curvature

face of bent specimen (initial space is 2 mm)

$$\phi = 2 \tan^{-1}\left(\frac{2}{r_b - W}\right): \text{bending angle for chord length of 4 mm}$$

4.4 Bending Moment and Bending Strain

a. Uniform bending test

Uniform bending tests were carried out, using the two methods illustrated in Fig. 15, and typical test results are shown in Fig. 14. The figure shows relation between bending moment at middle section of specimen and bending strain on the section, marks ● and ○ are observed values in the plane strain state and in the plane stress state respectively, and they agree quite well with the calculated results based on Tresca's yield condition.

b. Bending test under concentrated load

In this case, when the load is not small, we can not neglect effect of friction force F between supports and specimen on the bending moment.

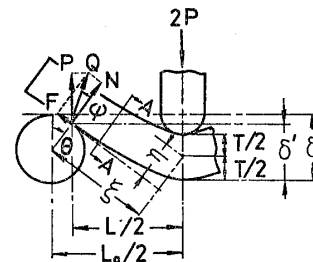


Fig. 19 Friction force on supports

Considering the friction force, the bending moment at middle span of the specimen is calculated from the following equations.

$$M = N\xi + F\eta$$

where

$$\left. \begin{aligned} N &= P/2 \sec \theta - F \tan \theta \\ \xi &= L/2 \cos \theta + (\delta' - T/2) \sin \theta \\ \eta &= L/2 \sin \theta - (\delta' - T/2) \cos \theta \end{aligned} \right\} \quad (17)$$

Fig. 20 shows relation between the friction force per unit breadth of the specimen F/B_0 and concentrated force $2P$ at middle span, and relation between the bending angle θ and angle of inclination ϕ of reaction force Q to

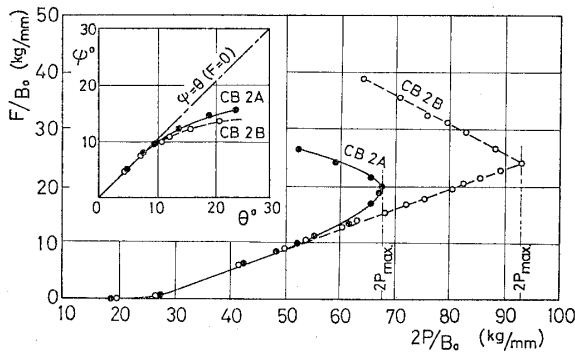


Fig. 20 Relation between friction force and concentrated load

the normal of the specimen at the support is also shown in the figure.

When $\theta \doteq \phi$, the friction force is nearly equal to zero, but if the bending angle θ exceeds 10 degree, the force increases in proportion to the load $2P$ and even after the load approached to its maximum value $2P_{max}$, the force increases continuously with increase of the bending deflection as shown in Fig. 20.

The friction force was determined from the following equation

$$F = E \frac{\epsilon_c + \epsilon_t}{2} B_0 T_0 \quad (18)$$

where E is Young's modulus and ϵ_t and ϵ_c are elastic circumferential strains measured with strain gages on convex and concave surface of the specimen at $A-A$ section shown in Fig. 19.

Relation between the bending moment with friction force correction and the bending strain obtained from results of the bending test agrees with that obtained from uniform bending test quite well, but when the friction force is neglected, a little difference is found between the two bending moment-strain curves.

4.5 Initiation of Bending Crack

Fig. 21 shows relation between circumferential bending strain at the crack $\epsilon_{\theta f}$ and initial thickness of specimen T_0 under uniform bending load. $2C$ is the crack length measured with magnifying-glass and dot-dash-lines show relation between maximum bending strain $\epsilon_{\theta max}$ and the thickness T_0 , and the strain $\epsilon_{\theta max}$ is the maximum strain determined from

combination of the plate thickness T_0 and head radius of mandrel R geometrically.

It can be seen from the figure that the bending strain at the crack $\epsilon_{\theta f}$ decreases with the increase of the plate thickness T_0 and converges to some minimum value and for the same crack length, the strain $\epsilon_{\theta f}$ in the plane strain state is about 40% smaller than that in the plane stress state.

In order to confirm the cause, strain and stress distribution in the two stress states were analysed by the theory derived in section 2. In the both states, the normal stress in radial direction σ_r on the surface of the specimen is zero and the stress gradient $d\sigma_r/dr$ in the vicinity of the surface is nearly equal to zero, then the stress σ_r can be assumed to be zero in the outermost layer of the bent specimen.

Fig. 22 shows relation between circumferential stress σ_θ and logarithmic bending strain $\bar{\epsilon}_\theta$ in the two stress states and relation between breadthwise stress σ_z and the strain $\bar{\epsilon}_\theta$ in the plane strain state.

Bending strain gradient $d\bar{\epsilon}_\theta/dr$ and bending stress gradient $d\sigma_\theta/dr$ in the outermost layer of the plate are shown in Fig. 23 in nondimensional forms.

As it is clear from the figure, there is no large difference in stress and strain gradient between two stress states, and obviously these gradients decrease with increase of plate thick-

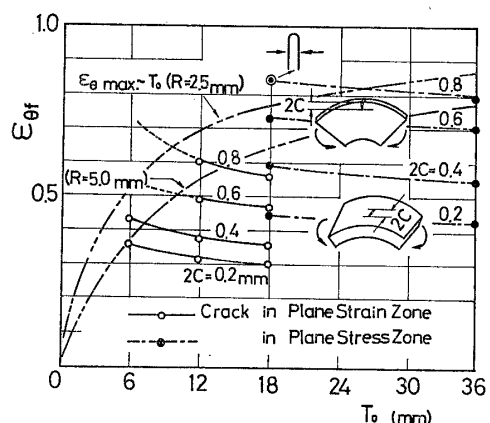


Fig. 21 Relation between nominal bending strain at the initiation of crack and plate thickness

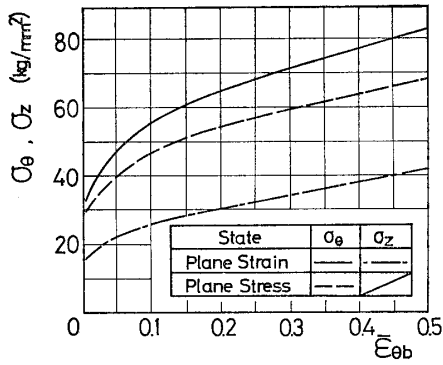


Fig. 22 Bending stress and strain on the surface of plate in the two stress state

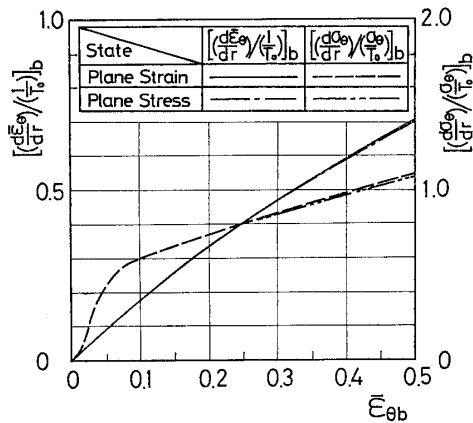


Fig. 23 Strain and stress gradients on the surface of plate

ness and tend to zero, then trend of the strain $\epsilon_{\theta f}$ and plate thickness T_0 curves in Fig. 21 may be explained.

In the next place, difference between magnitude of the strains $\epsilon_{\theta f}$ in the two stress states will be discussed. Stress condition on surface of the specimen in the plane strain state is two axial stress state and circumferential stress σ_θ and breadthwise stress $\sigma_z = \sigma_\theta/2$ are produced but in the plane stress state, there is only circumferential stress σ_θ and σ_z is equal to zero and moreover as it can be seen in Fig. 22, the stress σ_θ in the plane stress state is about fifteen percent smaller than that in the plane strain state. These facts may be considered to be the cause of the difference in the crack initiation strain $\epsilon_{\theta f}$ between the two stress state.

4.6 Bending Crack in the Plane Strain State

Since the first bending crack initiates always in the region of plane strain state unless breadth of the specimen is extremely small, mechanism of the crack initiation should be discussed in the plane strain state. Relation between range of the plane strain state \bar{b} observed in the two kinds of bending tests and breadth of the specimen b_0 or B_0 is shown in Fig. 24 and touched breadth of mandrel b' on the specimen under concentrated load is also shown in the figure.

Deformation of the specimen caused by uniform bending load tends to be saddle form but deformation of cross section of the specimen under concentrated load is restricted with the mandrel and the saddle type deformation is difficult to occur, therefore the range of the plane strain state of the specimen under concentrated load is wider than that under uniform bending load as seen in Fig. 24.

Fig. 25 shows relation between the bending strain at each crack length $2C$ and breadth of

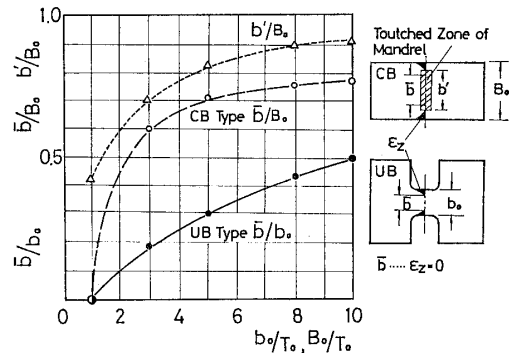


Fig. 24 Region of the plane strain state

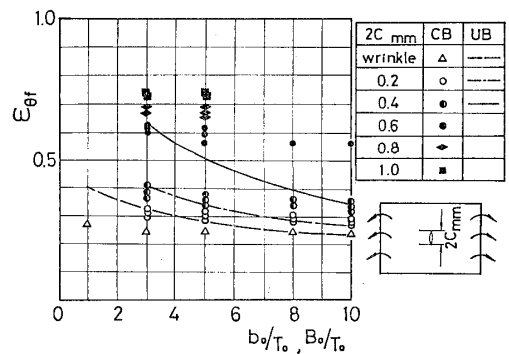


Fig. 25 Relation between crack initiation and shape of specimen

the specimen. The bending strains decrease with increase of breadth of the specimen and converge to some constant value and in case of concentrated loading test, the strains converge when breadth to thickness ratio of the specimen is larger than 5 and in case of uniform bending test, the strains converge to the same value as in concentrated loading test when the ratio exceeds 8.

Fig. 26 shows relation between circumferential strain $\epsilon_{\theta c}$ and bending angle 2θ , and these curves converge to the maximum value which is determined from combination of head radius of mandrel R and thickness of the specimen T_0 geometrically and the maximum value is given by the equation $\epsilon_{\theta \max} = (T_0/2)/(R + T_0/2)$.

Relation between the circumferential strain $\epsilon_{\theta c}$ and radius of convex surface of the specimen r_b and relation between the bending angle 2θ and the radius r_b are shown in Fig. 27.

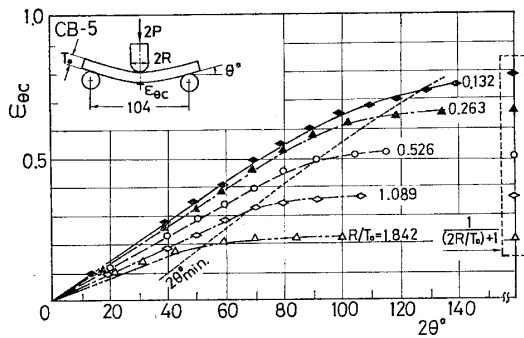


Fig. 26 Relation between circumferential strain and bending angle

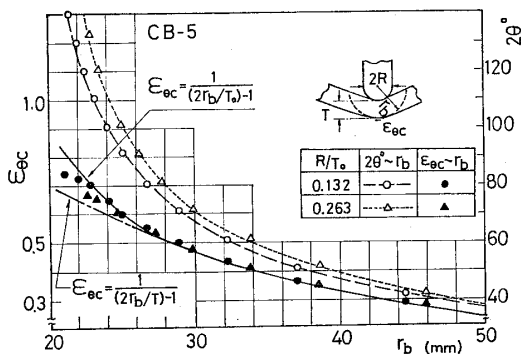


Fig. 27 Relation between bending angle or circumferential strain and radius of mandrel

The strain is given by the formula $\epsilon_{\theta c} = (T/2)/(r_b - T/2)$ approximately, where T is thickness of the bent specimen and when the strain is smaller than 0.4, we can use initial thickness of the specimen T_0 instead of T in the formula but when the strain is larger than 0.4, reduction in the thickness due to pressure of the mandrel can not be neglected.

5. New Proposal for Bending Test Method of Thick Steel Plate

5.1 Loading

Bending tests have been carried out to examine the ductility of materials and most of them are concentrated loading tests because of its simplicity.

Uniform bending test is an ideal method but it needs large size of specimen and a little complicated apparatus, therefore this test is not practical for industrial purposes.

According to the results of our tests, effect of friction force between the specimen and supports on the bending moment can not be neglected but that on the initiation of bending crack may be neglected, because axial strain caused by the friction force is negligibly small compared with the bending strain.

By the above mentioned reason, we propose a concentrated loading test for industrial test of materials.

5.2 Dimension of Specimen

As in Fig. 25, the bending strain at the crack $\epsilon_{\theta f}$ decreases with increase of the ratio of breadth to thickness of the specimen B_0/T_0 and converge to a constant value when the ratio B_0/T_0 exceeds 5, accordingly the ratio of bending specimen is advisable to be more than 5.

The friction force between the specimen and supports decreases in proportion to span between the supports but as effect of the force on the initiation of bending crack is negligibly small, the span L_0 needs only to satisfy the following condition, that is, $L_0 \geq 2(R + T_0) + D$, where R is head radius of mandrel and D is diameter of roller support.

5.3 Head Radius of Mandrel

The maximum bending strain $\epsilon_{\theta \max}$ is de-

terminated from ratio of the radius of mandrel to the thickness of specimen R/T_0 as shown in Fig. 26 therefore the radius R should be selected correspondingly to the given maximum strain $\epsilon_{\theta_{max}}$.

5.4 Bending Angle

If the maximum strain $\epsilon_{\theta_{max}}$ is given, the corresponding ratio R/T_0 and the minimum bending angle θ_{min} needed to produce the given strain $\epsilon_{\theta_{max}}$ can be decided from curves shown in Fig. 28.

5.5 Measurement of Bending Strain

When the maximum strain $\epsilon_{\theta_{max}}$ is given, the corresponding ratio R/T_0 and the minimum bending angle θ_{min} is determined as mentioned above, however if the crack initiates before the bending angle θ reaches to the minimum value θ_{min} , the bending strain at the crack can be estimated from $2\theta - r_b$ curves in Fig. 27 and the radius of convex

surface of the bent specimen r_b can be easily measured with the simple device shown in Fig. 18.

5.6 Method of Bending Test

Summing up the above mentioned factors, we propose the following bending test method for industrial use.

Loading; concentrated load test as shown in Fig. 29.

- Breadth of specimen; $B_0 > 5T_0$
- Length of specimen; $L > \pi\left(R + \frac{T_0}{2}\right) + 2C$
- Span of support; $L_0 > 2(R + T_0) + D$
- Head radius of mandrel; $R = \frac{T_0}{2}\left(\frac{1}{\epsilon_{\theta_{max}}} - 1\right)$
- Point angle of mandrel; $\phi > \theta_{min}$

where D is radius of the roller support and is advisable to be about 30 mm for reduction of friction force, and C is a constant value and is about 20 mm when clinometer is used for the measurement of bending angle.

6. Conclusion

In order to analyse mechanism of large deformation under uniform bending load, a new analytical method was derived, and test results were compared to calculated values with good agreement.

Using the method, strain and stress distributions in specimens under uniform bending loads of different magnitudes were analysed and existence of unloading phenomenon near the neutral plane of the specimen was confirmed.

On the other hand, bending tests under concentrated load were carried out and effect of friction force at support and shape of specimen on the initiation of bending crack were clarified, and relation between maximum bending strain and head radius of mandrel and relation between bending angle and bending strain etc. were obtained.

Based on these results, a new bending test method was proposed.

A summary of the results is shown below.

1) The first bending crack initiates always in the middle part of plate where stress condition is the plane strain state, although bending

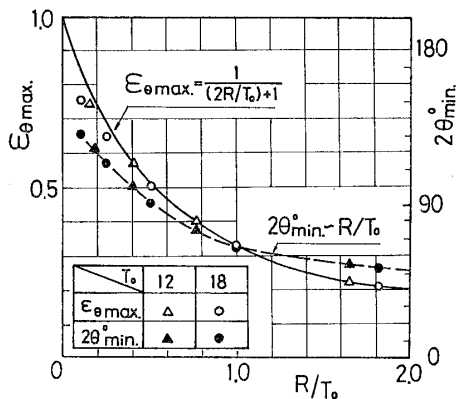


Fig. 28 Relation between min. bending angle or max. circumferential strain and radius of mandrel

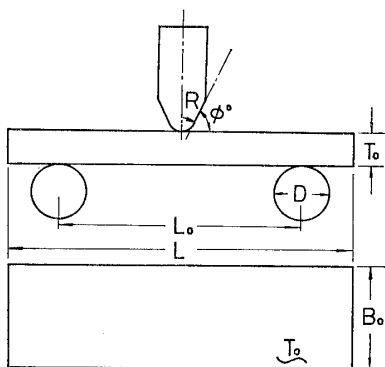


Fig. 29 Bending test under concentrated load

strain in this part is smaller than that in edge of the plate.

2) Effect of friction force between specimen and support on bending moment can not be neglected especially in case of bending test with short span but that on the initiation of bending crack may be neglected, because axial strain caused by the friction force is negligibly small compared with bending strain.

3) Relation between bending moment and bending strain on surface of plate in the plane strain state can be analysed by the method based on Tresca's yield condition with sufficient accuracy, but the method based on Mises' yield condition estimates the strain hardening effect of material on the bending moment excessively.

4) For the same bending strain on convex surface of plate, bending moment in the plane stress state is a little smaller than that in the plane strain state.

5) On relation between bending radius and bending strain or bending angle, there is no distinct difference between that two stress states.

6) Strain gradient on surface of plate in the plane stress state is nearly equal to that in

the plane strain state but stress gradient in the former state is a little smaller than that in the latter state.

Acknowledgement

Some part of this work was carried out as one of the researches of technical committee established in Society of Steel Construction of Japan and grateful acknowledgement is made to emeritus professor Okumura who is chairman of the committee, and the authors express their deep thanks to emeritus professor Terazawa for his kind guidance, and to the members of the committee for their valuable discussion.

References

- 1) G. SANGDAHL and G. SACHS; An Investigation at the Stress and Strain State Occuring in Bending Rectangular Bars, Proc. of Experimental Stress Analysis, Vol. 6, Part 1, (1948) p. 1
- 2) R. HILL; The Mathematical Theory of Plasticity, Oxford at The Clarendon Press (1950)
- 3) B. SCHAFFER and R. HOUSE; The Significance Zero Shear Stress in The Pure Bending of Wide Curved Bar, J. of Aeronautical Science, Vol. 24 (1957) p. 307